

Nonlinear photoncurrent in transition metal dichalcogenide with warping term under illuminating of light

Guo-Bao Zhu(朱国宝), Hui-Min Yang(杨慧敏), and Yun-Hai Zhang(张运海)
Citation: Chin. Phys. B, 2021, 30 (**3**): 037301. DOI: 10.1088/1674-1056/abc53c
Journal homepage: http://cpb.iphy.ac.cn; http://iopscience.iop.org/cpb

What follows is a list of articles you may be interested in

Electronic structure of molecular beam epitaxy grown 1T'-$MoTe_2$ film and strain effect

Xue Zhou(周雪), Zeyu Jiang(姜泽禹), Kenan Zhang(张柯楠), Wei Yao(姚维), Mingzhe Yan(颜明哲), Hongyun Zhang(张红云), Wenhui Duan(段文晖), Shuyun Zhou(周树云)
Chin. Phys. B, 2019, 28 (**10**): 107307. DOI: 10.1088/1674-1056/ab43ba

Electronic and magnetic properties of CrI_3 nanoribbons and nanotubes

Ji-Zhang Wang(王吉章), Jian-Qi Huang(黄建啟), Ya-Ning Wang(王雅宁), Teng Yang(杨腾), Zhi-Dong Zhang(张志东)
Chin. Phys. B, 2019, 28 (**7**): 077301. DOI: 10.1088/1674-1056/28/7/077301

Room-temperature infrared photodetectors with hybrid structure based on two-dimensional materials

Tiande Liu(刘天德), Lei Tong(童磊), Xinyu Huang(黄鑫宇), Lei Ye(叶镭)
Chin. Phys. B, 2019, 28 (**1**): 017302. DOI: 10.1088/1674-1056/28/1/017302

Tunable charge density wave in TiS_3 nanoribbons

Ce Huang(黄策), Enze Zhang(张恩泽), Xiang Yuan(袁翔), Weiyi Wang(王伟懿), Yanwen Liu(刘彦闻), Cheng Zhang(张成), Jiwei Ling(凌霁玮), Shanshan Liu(刘姗姗), Faxian Xiu(修发贤)
Chin. Phys. B, 2017, 26 (**6**): 067302. DOI: 10.1088/1674-1056/26/6/067302

Au and Ti induced charge redistributions on monolayer WS_2

Zhu Hui-Li, Yang Wei-Huang, Wu Ya-Ping, Lin Wei, Kang Jun-Yong, Zhou Chang-Jie
Chin. Phys. B, 2015, 24 (**7**): 077301. DOI: 10.1088/1674-1056/24/7/077301

Nonlinear photoncurrent in transition metal dichalcogenide with warping term under illuminating of light*

Guo-Bao Zhu(朱国宝), Hui-Min Yang(杨慧敏)†, and Yun-Hai Zhang(张运海)‡

School of Physics and Electronic Engineering, Heze University, Heze 274015, *China*

(Received 23 August 2020; revised manuscript received 3 October 2020; accepted manuscript online 28 October 2020)

We investigate the photoconductivities of injection current and the shift current in transition metal dichalcogenide with warping term in the presence of sublattice potential and spin orbit coupling. The system shows the valley photoconductivities of injection current and the photoconductivities of shift current. It is found that the warping term and the geometric tensor play a critical role in the system, which are responsible for the photoconductivities. Due to the interplay between the sublattice potential and the spin orbit coupling, the photoconductivities can be tuned. Furthermore, the effect of warping term on geometric tensor and the amplitude of the photoconductivities are also discussed.

Keywords: photoconductivity, transition metal dichalcogenide, warping term

PACS: 73.43.–f, 78.20.–e **DOI:** 10.1088/1674-1056/abc53c

1. Introduction

With the rapid progress in synthesizing and characterizing, monolayer transition metal dichalcogenide (TMDC) has become a powerful candidate for its practical applications in future nanophotonic devices and technology. Monolayer TMDC is a direct band gap semiconductor. The inversion asymmetric crystal structure leads to spin valley coupling and valley contrasting Berry curvature.[1–4] Therefore, monolayer TMDC is a suitable candidate for optical manipulations, and provides access to many optoelectronic applications. It has been predicted that both valley Hall and spin Hall conductivities can be achieved in monolayer TMDC by circularly and linearly polarized light.[5–8] When the spin orbit coupling and warping term are absent, optical absorption in monolayer TMDC has been studied.[9,10] Furthermore, the ultrafast valley relaxation dynamics in monolayer MoS_2 was probed by non-equilibrium optical technique.[11] The effect of intense femtosecond laser excitation on the monolayer MoS_2 has been studied.[12] Moreover, femtosecond valley polarization and topological resonances in TMDC were studied by a single cycle of a strong circularly polarized optical field with duration of a few femtoseconds.[13] Photocurrent in TMDC also has been investigated.[14,15] However, the nonlinear response on external field in TMDC has been poorly understood.

We focus on the second-order nonlinear response, which has received increasing attention as a way to probe the topological properties of materials. There are a variety of second-order nonlinear response including inject current, shift current, nonlinear Hall effect, and harmonic generation. The injection and shift mechanisms are two important ones of term. They are resulted from the transition of electron velocity and the transition of electron position during the optical excitation, respectively. They are second-order nonlinear optical effect, which has been attracting increasing interest and intensively investigated theoretically and experimentally.[16–27] Due to time-reversal symmetry breaking in magnetic systems, linearly polarized light can generate injection currents. An unusual photogalvanic effect has been predicted on the topological insulator surface when its semimetallic electronic spectrum is modified by an adjacent ferromagnet.[28] Ogawa *et al.*[29] demonstrated the generation of large zero-bias photocurrent in magnetic topological insulator thin films on mid-infrared photoexcitation. The combination of inversion symmetry breaking and finite tilts of the Weyl spectra can lead to significant photocurrents in three-dimensional Weyl semimetals.[30] The shift current is a steady-state photocurrent generated in the materials without inversion symmetry, originating from the geometric Berry phase of the constituting electron bands. The shift current has been proved to lead the ground breaking discoveries in Weyl semimetals,[31] tungsten disulfide nanotubes,[32] and silicon.[33] In experiment, the inject current can be detected by illuminating optical field,[34–36] and the shift current can be detected by short-circuit current measurements.[37,38] They have potential applications in energy harvesting, photon detection, nonlinear electronics, and quantum-confined spintronic devices.

Given these backgrounds, we present detail of studying on the photoncurrent in TMDC induced by a nonlinear optical interaction due to the illuminating of light. We focus on the injection and shift mechanisms. In TMDC, the warping term induces important modification on geometric tensor, which depends on valley and spin index. Furthermore, the photoncur-

*Project supported by the National Natural Science Foundation of China (Grant No. 11504095) and the Science and Technology Program for Institutions of Higher Learning in Shandong Province, China (Grant No. J18KA224).

†Corresponding author. E-mail: yangyhm@163.com

‡Corresponding author. E-mail: wlxzyh@163.com

© 2021 Chinese Physical Society and IOP Publishing Ltd

rent in TMDC is governed by warping term and geometric tensor.

This paper is organized as follows. We firstly describe the model with warping term, and analyze band structure in Section 2, and present the results for Berry curvature and geometric tensor in Section 3. In Section 4, we present the results of the injection current and shift current. We analyze the effect of warping on geometric tensor, the valley photoconductivities of injection current, and the photoconductivities of shift current. Finally, we give a brief conclusion in Section 5.

2. Model

The effective two-band model of monolayer TMDC with warping term around the K and K' valleys (labeled by $\eta = \pm 1$ respectively) is[1–4]

$$H = \eta v k_x \sigma_x + v k_y \sigma_y + \frac{\Delta}{2}\sigma_z - \eta s \frac{\lambda}{2}(\sigma_z - 1) + \kappa(k_x^2 - k_y^2)\sigma_x - 2\eta\kappa k_x k_y \sigma_y, \quad (1)$$

where v is the Fermi velocity, $k_{x,y}$ are components of the momentum measured relative to the K/K' point, $\sigma_{x,y,z}$ are the Pauli matrices associated with the sublattice pseudospin, Δ is responsible for opening the band gap, 2λ is the spin splitting at the valence band top caused by the spin orbit coupling, and s is the index for spin. Here κ is responsible for the warping term, which is resulted from the lattice structure in TMDC.[1,2] Moreover, the warping term in honeycomb lattice can be tuned by Rashba spin-orbit coupling[39,40] or strain.[41] All energies are measured in units of v in this work.

For a two-band system, the Hamiltonian can always be expressed in terms of the Pauli matrices as

$$H = d_0 \boldsymbol{I} + \boldsymbol{d}\cdot\hat{\boldsymbol{\sigma}}. \quad (2)$$

In TMDC, $\boldsymbol{d} = (d_x(\boldsymbol{k}), d_y(\boldsymbol{k}), d_z(\boldsymbol{k}))$, $\hat{\boldsymbol{\sigma}} = (\sigma_x, \sigma_y, \sigma_z)$, $d_0 = \eta s\frac{\lambda}{2}$, $d_x(\boldsymbol{k}) = \eta v k_x + \kappa(k_x^2 - k_y^2)$, $d_y(\boldsymbol{k}) = v k_y - 2\eta\kappa k_x k_y$, $d_z(\boldsymbol{k}) = \frac{\Delta}{2} - \eta s\frac{\lambda}{2}$, and $\boldsymbol{I}$ is the rank-2 unit matrix. The corresponding eigenvalues and eigenvectors are

$$E_n = d_0 + (-1)^n\sqrt{d_x^2 + d_y^2 + d_z^2}, \quad (3)$$

and

$$|n\rangle = \mathrm{e}^{(-1)^n \mathrm{i}\frac{\gamma}{2}}\left[\sin\left(\frac{\theta}{2} + \pi\frac{n-1}{2}\right)\mathrm{e}^{\mathrm{i}\frac{\gamma}{2}}, -\cos\left(\frac{\theta}{2} + \pi\frac{n-1}{2}\right)\mathrm{e}^{-\mathrm{i}\frac{\gamma}{2}}\right]^{\mathrm{T}}, \quad (4)$$

where $n = 1, 2$ denote the valence (conduction) band, superscript T denotes the transpose of the matrix, $\tan\theta = \sqrt{d_x^2 + d_y^2}/d_z$, and $\tan\gamma = d_y/d_x$. In order to show the effect of the warping term, we plot the energy contours of valence band without and with the warping term in Figs. 1(a) and 1(b) for $\eta = 1$ and $s = 1$ at fixed $\Delta = 0.5v$ and $\lambda = 0.1v$, respectively. When the warping term is present, the warping term mostly deforms Fermi surfaces, which are significantly trigonal-warped valence band. Furthermore, the bands have a threefold rotational symmetry. Moreover, Figs. 1(c) and 1(d) show the energy bands along $k_y = 0$ without and with the warping term, respectively. The effect of the warping term in the valence band is different from that in the conduction band due to the electron-hole asymmetry induced by $s\eta\lambda/2$. Due to the change of energy band dispersion, the corresponding group velocity is modified. Therefore, the warping term induces important modifications on Berry curvature and geometric tensor, and the effect of the warping term on Berry curvature and geometric tensor will be included in the next section. This means that the warping term will play an important role in the electronic transport properties of TMDC.

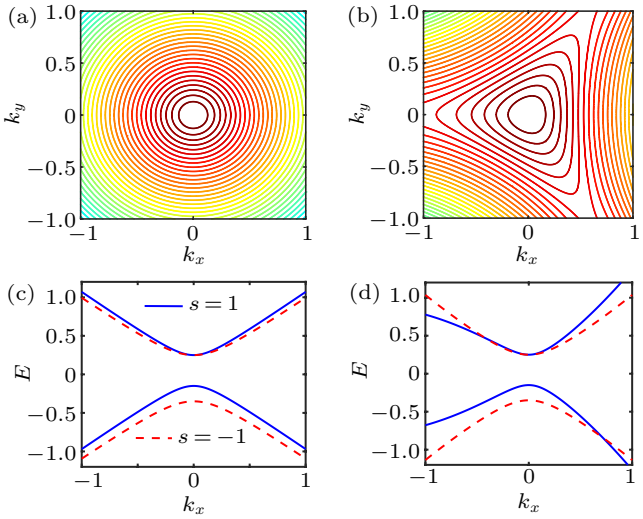


Fig. 1. Contours plot of the corresponding valence band for monolayer TMDC in units of v without (a) and with (b) the warping term for $\eta = 1$ and $s = 1$ at fixed $\Delta = 0.5v$ and $\lambda = 0.1v$. The energy bands along $k_y = 0$ without (c) and with (d) the warping term. The blue solid lines denote spin-up bands and the red dashed lines correspond to spin-down bands.

3. Berry curvature and geometric tensor

In this section, we present the calculated results for Berry curvature and geometric tensor based on the following equations. Due to the good quantum numbers of spin and valley index, the corresponding Berry curvature in momentum-space for spin s and valley η component of the system is calculated by[42]

$$\Omega_n(\eta, s)(\boldsymbol{k}) = -\sum_{n'\neq n}\frac{2\mathrm{Im}\langle n|\hat{v}_x|n'\rangle\langle n'|\hat{v}_y|n\rangle}{(E_{n'} - E_n)^2}. \quad (5)$$

The summation is taken over all the occupied bands blow the bulk gap, and $\hat{v}_{x(y)}$ is the velocity operator along $x(y)$ direction. For our system, straightforward calculations show that the valley- and spin-dependent Berry curvature is

$$\Omega(\eta, s)(\boldsymbol{k}) = \eta\frac{\Delta - \eta s\lambda}{4|\boldsymbol{d}|^3}(v^2 - 4\kappa^2 k^2). \quad (6)$$

In Fig. 2, we plot the Berry curvatures of valence band in 2D plane for spin-up electron state in monolayer TMDC around the two valleys in the absence/presence of the warping term. The corresponding Berry curvatures for spin-down electron states can be obtained by time reversal symmetry. Berry curvature has opposite signs in opposite valleys for the spin-up energy band. The Berry curvatures decay rapidly, and eventually vanish away from the valleys. In the absence of the warping term, Figs. 2(a) and 2(c) show that the Berry curvatures only depend on the module of k, which can be confirmed by Eq. (6). The Berry curvatures are prominently warped in the presence of the warping term. Therefore, the warping term leads to significant corrections to the magnitude of the Berry curvatures, which is dependent on spin (s) and valley index (η). The spin and valley resolved intrinsic Hall conductance can be calculated from the Berry curvature directly. Therefore, the spin and valley Hall conductance can be tuned by controlling the warping term.[43] On the other hand, the symmetry of our system and Berry curvatures are C_{3v} when the trigonal warping term is included. Thus, the nonlinear Hall effect in warped TMDC is absent.[44]

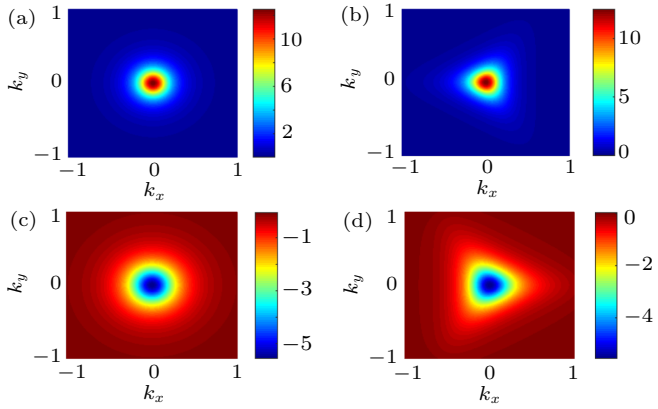


Fig. 2. Berry curvatures of valence band for monolayer TMDC for $s = 1$ at fixed $\Delta = 0.5v$ and $\lambda = 0.1v$. Here (a) and (b) are Berry curvatures without and with the warping term ($\kappa = 0.4$) for valley $\eta = 1$; (c) and (d) are Berry curvatures without and with the warping term ($\kappa = 0.4$) for valley $\eta = -1$.

Next, we study the warping effect on the geometric tensor. The geometric tensor is defined as[45]

$$g_{aa}(\eta, s) = \sum_{n' \neq n} \frac{\mathrm{Re}\langle n|\hat{v}_a|n'\rangle\langle n'|\hat{v}_a|n\rangle}{(E_{n'} - E_n)^2}. \tag{7}$$

Based on the eigenvectors (Eq. (4)) of our system, the valley- and spin-dependent geometric tensor in the valence band is obtained as follows:

$$g_{aa}(\eta, s)(\boldsymbol{k}) = -\frac{1}{4}\left[(\partial_a\theta)^2 + \sin^2\theta(\partial_a\gamma)^2\right]. \tag{8}$$

The geometric tensor distribution without (a)/(c) and with (b)/(d) the warping term are show in Fig. 3 for $s = 1$ at fixed $\Delta = 0.5v$ and $\lambda = 0.1v$, respectively. In contrast to that of Berry curvatures, the geometric tensors have the same signs at opposite valleys for the spin-up energy band. When the warping term is absent, we observe that the geometric tensors are peaked at the coordinate origin. Due to the warping term, the peaks will shift and split. Furthermore, the amplitudes of the peaks without and with the warping term are related to the valley index, which can be confirmed by the definitions of θ and γ. The amplitudes of the geometric tensor with or without the warping term in opposite valleys are different. Therefore, TMDC can be as a candidate for pseudospintronic (valley) devices, and the warping term will lead to the important modifications of physical quantity depending on geometric tensors. Moreover, the pseudospintronic (valley) transport should be studied due to the difference of the geometric tensor between the two valleys.

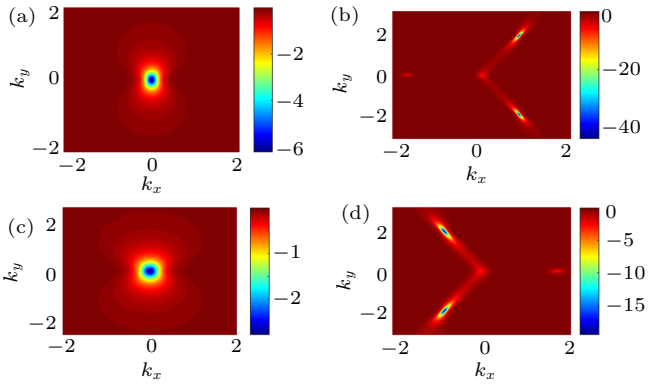


Fig. 3. Geometric tensor g_{xx} for monolayer TMDC without (a)/(c) and with (b)/(d) the warping term for $s = 1$ at fixed $\Delta = 0.5v$ and $\lambda = 0.1v$. Here (a) and (b) are the geometric tensors without and with the warping term ($\kappa = 0.4$) for valley $\eta = 1$; (c) and (d) are the geometric tensors without and with the warping term ($\kappa = 0.4$) for valley $\eta = -1$.

4. Injection current and shift current

In this section, we investigate the injection current and shift current, which are second-order optical effect with the induced direct current proportional to the square of electric field. For electric field at frequency ω, the photoconductivity of injection current and shift current are given by[16,26]

$$\sigma_{\mathrm{ic}}^{cab}(\omega) = \frac{2\tau\pi e^3}{\hbar}\int\frac{\mathrm{d}^2k}{(2\pi)^2}\sum_{nm} f_{nm} r^a_{nm} r^b_{nm} \Delta^c_{nm}\delta(\hbar\omega - E_{mn}), \tag{9}$$

$$\sigma_{\mathrm{sc}}^{cab}(\omega) = \frac{2\pi e^3}{\hbar}\int\frac{\mathrm{d}^2k}{(2\pi)^2}\sum_{nm} f_{nm} r^a_{nm} r^b_{nm} R^{cb}_{nm}\delta(\hbar\omega - E_{mn}), \tag{10}$$

where the summation is taken over all Bloch bands, $E_{mn} = E_m - E_n$; $f_{nm} = E_n - E_m$ is the difference of Fermi occupations with the Fermi–Dirac distribution function $f_n = 1/(1 + \mathrm{e}^{(E_n - E_F)/k_\mathrm{B}T})$, T is the temperature, k_B is the Boltzmann constant, $r^b_{nm} = \mathrm{i}\langle n|\partial_\mathrm{b} m\rangle$ for $m \neq n$ is inter-band Berry connection and is the intra-band Berry connection for band $m = n$, with $\partial_\mathrm{b} = \partial/\partial k_\mathrm{b}$ and $|n\rangle$ being the eigenstate of energy band E_n. $\Delta^a_{nm} = v_{nn} - v_{nm}$ is the group velocity difference of bands m and n. $R^{ab}_{nm} = \partial_a\phi^b_{nm} + r^a_{nn} - r^a_{mm}$ is the shift vector, and ϕ^b_{nm} is the phase factor of the Berry connection r^b_{nm}.

In this work, we focus on the components of photoconductivity $\sigma_{\rm ic}^{xaa}(\omega,\eta,s)$ and $\sigma_{\rm sc}^{yaa}(\omega,\eta,s)$ $(a=x,y)$. For our system,

$$\sigma_{\rm ic}^{caa}(\omega,\eta,s) = \frac{\tau\pi e^3}{\hbar}\int\frac{d^2k}{(2\pi)^2}\sum_{nm} f_{nm}g_{aa}\Delta_{nm}^{c}\delta(\hbar\omega-E_{mn}), \quad (11)$$

$$\sigma_{\rm sc}^{caa}(\omega,\eta,s) = \frac{\pi e^3}{\hbar}\int\frac{d^2k}{(2\pi)^2}\sum_{nm} f_{nm}g_{aa}R_{nm}^{ca}\delta(\hbar\omega-E_{mn}), \quad (12)$$

According to the eigenvectors (Eq. (4)), a straightforward calculation shows that the photoconductivity of injection current at zero temperature is

$$\begin{aligned}&\sigma_{\rm ic}^{xxx}(\omega,\eta,s)\approx-\sigma_{\rm ic}^{xyy}(\omega,\eta,s)\\ &=\frac{16\tau\pi e^3}{\hbar^3\omega^2[\hbar^2\omega^2-4d_z^2]}\int\frac{{\rm d}^2k}{(2\pi)^2}\frac{\partial|\boldsymbol{d}|}{\partial k_x}\delta(\hbar\omega-2|\boldsymbol{d}|)\\ &\times\left[|\hat{e}_z\cdot\boldsymbol{d}\times\partial_x\boldsymbol{d}|^2+\frac{d_z^2}{\hbar^2\omega^2}|\partial_x d^2|^2\right],\end{aligned} \quad (13)$$

while $\sigma_{\rm ic}^{yyy}(\omega,\eta,s)=\sigma_{\rm ic}^{yxx}(\omega,\eta,s)=0$; $d=|\boldsymbol{d}|=\sqrt{d_x^2+d_y^2+d_z^2}$. In Fig. 4, we plot the valley photoconductivity of injection current $\sigma_{\rm V,ic}^{xxx}(\omega)=\sum_{\eta s}\eta\sigma_{\rm ic}^{xxx}(\omega,\eta,s)$ as a function of ω at $\delta=0.1$ and $\lambda=0.4$ for varying κ, while $\sigma_{\rm ic}^{xxx}(\omega)=\sum_{\eta s}\sigma_{\rm ic}^{xxx}(\omega,\eta,s)\approx 0$. This is due to the time reversal symmetry of the energy bands and the same signs of the geometric tensors at opposite valleys. When the warping term is absent, the valley photoconductivity is zero. When ω locates at the top of first valence band, $\sigma_{\rm V,ic}^{xxx}(\omega)$ emerges suddenly, and decreases with the ω. When ω sweeps the top of the second valence band, $\sigma_{\rm V,ic}^{xxx}(\omega)$ shows a discontinuous behavior, and then decreases with the ω. The two positions of the peaks locate at top of the two valence bands. Finally, $\sigma_{\rm V,ic}^{xxx}(\omega)$ disappears at larger ω. Moreover, the amplitude of $\sigma_{\rm V,ic}^{xxx}(\omega)$ increases along with varying κ.

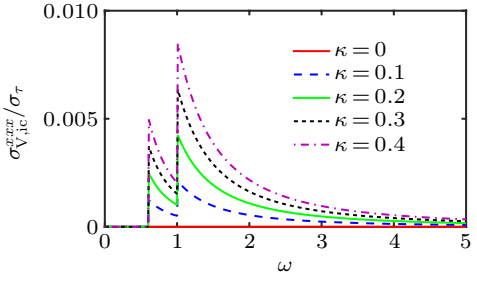


Fig. 4. Photoconductivity of injection current $\sigma_{\rm V,ic}^{xxx}$ dependence on ω in units of $\sigma_\tau=\tau e^3/\hbar$ at $\delta=0.1v$ and $\lambda=0.4v$ for $\kappa=0$, 0.1, 0.2, 0.3, and 0.4, respectively.

For the shift current, the photoconductivity at zero temperature is

$$\begin{aligned}&\sigma_{\rm sc}^{yyy}(\omega,\eta,s)\approx-\sigma_{\rm sc}^{yxx}(\omega,\eta,s)\\ &=\frac{4\pi e^3}{\hbar^4\omega^3}\int\frac{{\rm d}^2k}{(2\pi)^2}v\kappa(\Delta-\eta s\lambda)\delta(\hbar\omega-2|\boldsymbol{d}|),\end{aligned} \quad (14)$$

while $\sigma_{\rm sc}^{xxx}(\omega,\eta,s)=\sigma_{\rm sc}^{xyy}(\omega,\eta,s)=0$. Based on Eq. (14), the photoconductivity of shift current is determined by the warping term and it can be tuned by the interplay between the sublattice potential and spin orbit coupling. Figure 5 shows the band edge shift current $\sigma_{\rm sc}^{yyy}(\omega)=\sum_{\eta s}\sigma_{\rm sc}^{yyy}(\omega,\eta,s)$ as a function of ω at $\delta=0.1$ and $\lambda=0.4$ for varying κ, while $\sigma_{\rm V,sc}^{yyy}(\omega)=\sum_{\eta s}\eta\sigma_{\rm sc}^{yyy}(\omega,\eta,s)=0$. In the presence of the warping term, nonzero $\sigma_{\rm sc}^{yyy}(\omega)$ emerges suddenly at the top of the first valence band, and decreases with the ω. When ω sweeps the top of second valence band, $\sigma_{\rm sc}^{yyy}(\omega)$ shows a sign-reversal behavior. Finally, $\sigma_{\rm sc}^{yyy}(\omega)$ increases with ω, and disappears at larger ω. Moreover, the amplitude of $\sigma_{\rm sc}^{yyy}(\omega)$ can be controlled by changing κ.

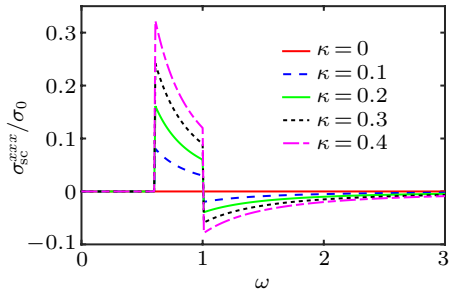


Fig. 5. Photoconductivity of shift current $\sigma_{\rm sc}^{yyy}$ dependence on ω in units of $\sigma_0=e^3/\hbar$ at $\delta=0.1v$ and $\lambda=0.4v$ for $\kappa=0$, 0.1, 0.2, 0.3, and 0.4, respectively.

Based on the results of the photoconductivities of inject and shift current, we can find that the warping term is playing an essential role in the nonlinear transport properties of materials. In TMDC, the warping term is due to the intrinsic lattice structure, which is different from the other materials. In graphene, the system shows the warped band structure when the Rashba spin-orbit coupling is stronger than the intrinsic spin-orbit coupling.[39] Considering a uniform uniaxial strain, graphene will has anisotropic warping term.[41] When the strength of the Rashba SOC becomes comparable to the hopping energy, silicene shows a warped low-energy Hamiltonian.[40]

5. Conclusions

In conclusion, we have studied the photoconductivities of injection current and the shift current in transition metal dichalcogenide with the warping term in the presence of the sublattice potential and the spin orbit coupling. It is found that there are the valley photoconductivities of injection current and the photoconductivities of shift current in the system. Moreover, we find that the the photoconductivities are determined by warping term and geometric tensor, and controlled by the interplay between the sublattice potential and the spin orbit coupling. Our findings provide a way to control the nonlinear transport properties of materials, and a approach to detect the geometric tensor by nonlinear optical response.

References

[1] Kormányos A, Zólyomi V, Drummond N D, Rakyta P, Burkard G and Fal'ko V I 2008 *Phys. Rev. B* **88** 045416
[2] Liu G B, Shan W Y, Yao Y, Yao W and Xiao D 2008 *Phys. Rev. B* **88** 085433
[3] Xiao D, Liu G B, Feng W, Xu X and Yao W 2012 *Phys. Rev. Lett.* **108** 196802
[4] Ilić S, Meyer J S and Houzet M 2019 *Phys. Rev. B* **99** 205407
[5] Li Z and Carbotte J P 2012 *Phys. Rev. B* **86** 205425
[6] Cao T, Wang G, Han W, Ye H, Zhu C, Shi J, Niu Q, Tan P, Wang E, Liu B and Feng J 2012 *Nat. Commun.* **3** 887
[7] Tahir M, Manchon A and Schwingenschlögl U 2014 *Phys. Rev. B* **90** 125438
[8] Sengupta P and Bellotti E 2016 *Appl. Phys. Lett.* **108** 211104
[9] Berkelbach T C, Hybertsen M S and Reichman D R 2015 *Phys. Rev. B* **92** 085413
[10] Rukelj Z, Štrkalj A and Despoja V 2016 *Phys. Rev. B* **94** 115428
[11] Conte S D, Bottegoni F, Pogna E A A, De Fazio D, Ambrogio S, Bargigia I, D, Andrea C, Lombardo A, Bruna M, Ciccacci F, Ferrari A C, Cerullo G and Finazzi M 2015 *Phys. Rev. B* **92** 235425
[12] Su X, Jiang L, Wang F, Su G, Qu L and Lu Y 2017 *Appl. Phys. A* **123** 1
[13] Motlagh S A O, Wu J S, Apalkov V and Stockman M I 2018 *Phys. Rev. B* **98** 081406
[14] Lee H C 2017 *Phys. Rev. B* **95** 245102
[15] Enaldiev V V 2017 *Phys. Rev. B* **96** 235429
[16] Sipe J E and Shkrebtii A I 2000 *Phys. Rev. B* **61** 5337
[17] Young S M and Rappe A M 2012 *Phys. Rev. Lett.* **109** 116601
[18] Young S M, Zheng F and Rappe A M 2012 *Phys. Rev. Lett.* **109** 236601
[19] Cook A M, Fregoso B M, Juan F d, Coh S and Moore J E 2017 *Nat. Comm.* **8** 14176
[20] McIver J W, Hsieh D, Steinberg H, Jarillo-Herrero P and Gedik N 2012 *Nat. Nanotechnol.* **7** 96
[21] Yuan H, Wang X, Lian B, Zhang H, Fang X, Shen B, Xu G, Xu Y, Zhang S Cheng, Hwang H Y and Cui Y 2014 *Nat. Nanotechnol.* **9** 851
[22] Dhara S, Mele E J and Agarwal R 2015 *Science* **349** 726
[23] de Juan F, Grushin A G, Morimoto T and Moore J E 2017 *Nat. Commun.* **8** 1
[24] Morimoto T, Nakamura M, Kawasaki M and Nagaosa N 2018 *Phys. Rev. Lett.* **121** 267401
[25] Ji Z, Liu G, Addison Z, Liu W, Yu P, Gao H, Liu Z, Rappe A M, Kane C L, Mele E J and Agarwal R 2019 *Nat. Mater.* **18** 955
[26] Wang H and Qian X 2019 *Sci. Adv.* **5** 9743
[27] Sotome M, Nakamura M, Fujioka J, Ogino M, Kaneko Y, Morimoto T, Zhang Y, Kawasaki M, Nagaosa N, Tokura Y and Ogawa N 2019 *Proc. Natl. Acad. Sci. USA* **116** 1929
[28] Semenov Y G, Li X and Kim K W 2012 *Phys. Rev. B* **86** 201401
[29] Ogawa N, Yoshimi R, Yasuda K, Tsukazaki A, Kawasaki M and Tokura Y 2016 *Nat. Commun.* **7** 12246
[30] Chan C K, Lindner N H, Refael G and Lee P A 2017 *Phys. Rev. B* **95** 041104
[31] Ma J, Gu Q, Liu Y, Lai J, Yu P, Zhuo X, Liu Z, Chen J H, Feng J and Sun D 2019 *Nat. Mater.* **18** 476
[32] Zhang Y J, Ideue T, Onga M, Qin F, Suzuki R, A Zak, Tenne R, Smet J H and Iwasa Y 2019 *Nature* **570** 349
[33] Yang M M, Kim D J and Alexe M 2018 *Science* **360** 904
[34] Yuan H, Wang X, Lian B, Zhang H, Fang X, Shen B, Xu G, Xu Y, Zhang S C, Hwang H Y and Cui Y 2014 *Nat. Nanotech.* **9** 856
[35] Dhara S, Mele E J and Agarwal R 2015 *Science* **349** 726
[36] Ji Z, Liu G, Addison Z, Liu W, Yu P, Gao H, Liu Z, Rappe A M, Kane C L, Mele E J and Agarwa R 2019 *Nat. Mater.* **18** 955
[37] Osterhoudt G B, Diebel L K, Gray M J, Yang X, Stanco J, Huang X, Shen B, Ni N, Moll P J W, Ran Y and Burch K S 2019 *Nat. Mater.* **18** 471
[38] Nakamura M, Horiuchi S, Kagawa F, Ogawa N, Kurumaji T, Tokura Y and Kawasaki M 2017 *Nat. Commun.* **8** 281
[39] Rakyta P, Kormányos A and Cserti J 2010 *Phys. Rev. B* **82** 113405
[40] Ma D S, Yu Z M, Pan H and Yao Y 2018 *Phys. Rev. B* **97** 085416
[41] Battilomo R, Scopigno N and Ortix C 2019 *Phys. Rev. Lett.* **123** 196403
[42] Yao Y, Kleinman L, MacDonald A H, Sinova J, Jungwirth T, Wang D, Wang E and Niu Q 2004 *Phys. Rev. Lett.* **92** 037204
[43] Chen W, Zhou X, Liu P, Xiao X and Zhou G 2020 *Phys. Lett. A* **384** 126344
[44] Sodemann I and Fu L 2015 *Phys. Rev. Lett.* **115** 216806
[45] Bleu O, Solnyshkov D D and Malpuech G 2018 *Phys. Rev. B* **97** 195422